

# Kitaev materials beyond iridates: order by quantum disorder and Weyl magnons in rare-earth double perovskites

Fei-Ye Li<sup>1,\*</sup>, Yao-Dong Li<sup>2,\*</sup>, Yue Yu<sup>2,3</sup>, and Gang Chen<sup>2,3†</sup>

<sup>1</sup>*CAS Key Laboratory of Theoretical Physics, Institute of Theoretical Physics, Chinese Academy of Sciences, Beijing 100190, People's Republic of China*

<sup>2</sup>*State Key Laboratory of Surface Physics, Center for Field Theory and Particle Physics, Department of Physics, Fudan University, Shanghai 200433, People's Republic of China*

<sup>3</sup>*Collaborative Innovation Center of Advanced Microstructures, Nanjing, 210093, People's Republic of China*

(Dated: May 4, 2022)

Motivated by the experiments on the rare-earth double perovskites, we propose a generalized Kitaev-Heisenberg model to describe the generic interaction between the spin-orbit-entangled Kramers doublets of the rare-earth moments. We carry out a systematic analysis of the mean-field phase diagram of this new model. In the phase diagram, there exist large regions with a continuous  $U(1)$  or  $O(3)$  degeneracy. Since no symmetry of the model protects such a continuous degeneracy, we predict that the quantum fluctuation lifts the continuous degeneracy and favors various magnetic orders in the phase diagram. From this order by quantum disorder mechanism, we further predict that the magnetic excitations of the resulting ordered phases are characterized by nearly gapless pseudo-Goldstone modes. We find that there exist Weyl magnon excitations for certain magnetic orders. We expect our prediction to inspire further study of Kitaev physics, the order by quantum disorder phenomenon and topological spin wave modes in the rare-earth magnets and the systems alike.

## I. INTRODUCTION

There has been an intensive interest in the study of Kitaev materials<sup>1–15</sup>. Originally, Kitaev materials refer to honeycomb<sup>1,2,16,17</sup>, hyperhoneycomb<sup>9,18,19</sup>, harmonic honeycomb<sup>11</sup>, and hyperkagome iridates<sup>20–22</sup>, and more recently, have been extended to the new material  $\text{RuCl}_3$ <sup>23–25</sup>. In these systems, the magnetic ions are heavy elements like  $\text{Ir}^{4+}$  and  $\text{Ru}^{4+}$ , where the spin-orbit coupling (SOC) is quite strong. Due to the spin-orbit entanglement of the local moments, the interaction between them depends on the bond orientation<sup>1,21,26,27</sup>, and may involve a large Kitaev spin interaction<sup>1</sup>. Since Kitaev model<sup>28</sup> supports a robust quantum spin liquid ground state, one goal of exploring these systems is to realize the Kitaev spin liquid with a dominant Kitaev interaction. More generally, it is of great importance to understand the role of spin-orbit entanglement on the properties of a strongly correlated quantum many-body system<sup>29</sup>.

Since the Kitaev interaction<sup>1</sup>, or more precisely, the bond dependent spin interaction, is a natural consequence of the strong SOC<sup>21</sup>, its presence should go beyond iridates or ruthenates. The vast families of rare-earth magnets have never been explored along the line of Kitaev interaction. In fact, rare-earth moments have much stronger SOC than iridium or ruthenium<sup>30–38</sup>. The  $4f$  electrons are much more localized than the  $5d$  or  $4d$  electrons in iridates and ruthenates. Most often, the interaction between the local moments in the rare earth systems is merely restricted to the nearest neighbors, while the iridates or ruthenates may involve significant further neighbor interactions due to the extended electron wavefunctions<sup>39</sup>. Moreover, the rare-earth elements do not suffer from the neutron absorption issue that prevails in the study of iridates<sup>16,17</sup>. Because of the small

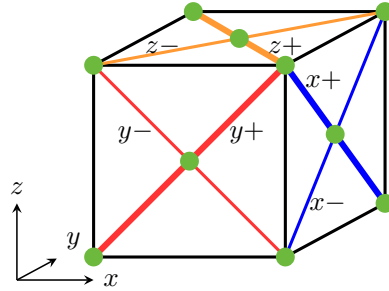


FIG. 1. (Color online.) The bond dependent interactions in the FCC lattice. We have marked the six distinct bond types  $\gamma\pm$  ( $\gamma = x, y, z$ ), that have the specific forms of bond-dependent interactions in Eq. 1. The inset is the global coordinate system that defines the spin components.

energy scale of the interaction, the external magnetic field and the inelastic neutron scattering could even be used to precisely determine the Hamiltonian of the rare-earth systems. All these advantages make the rare-earth systems ideal Kitaev materials.

In this paper, we turn from iridates to the rare-earth systems and explore the consequence of the spin-orbit entanglement and the Kitaev interaction in rare-earth double perovskites. Double perovskite ( $\text{A}_2\text{BB}'\text{O}_6$ ) is a very common system in which the magnetic ions  $\text{B}'$  form a face-centered-cubic (FCC) lattice<sup>26,27,40</sup>. Previously, the interplay of strong correlation and strong SOC has been explored for the  $4d$  and  $5d$  transition metal elements with partially filled  $t_{2g}$  shells<sup>26,27</sup>. It was pointed out that the strong spin-orbit entanglement gives a multipolar structure of the local moments and rich magnetic multipolar orders<sup>26,27</sup>. In contrast, the rare-earth electrons often experience substantial crystal electric field (CEF)

that splits the  $(2J+1)$ -fold degeneracy of the spin-orbit-entangled total moment  $\mathbf{J}$ . For a half-integer moment  $J$ , the CEF ground state is a Kramers' doublet whose degeneracy is protected by the time reversal symmetry. Often, the CEF gap is much larger than the temperature scale and exchange interaction in the system, and the low-temperature magnetic properties are fully captured by the ground state doublets that are modeled by pseudospin-1/2 local moments.

For the rare-earth double perovskites ( $\text{Ba}_2\text{LnSbO}_6$ ,  $\text{Ln} = \text{rare earths}$ )<sup>40-45</sup>, we propose a generic model on the FCC lattice that describes the nearest-neighbor interaction between the Kramers' doublet local moments. This generic model involves the Heisenberg interaction, the Kitaev interaction, and an additional crossing exchange that is symmetric in two pseudospin components. In the mean-field phase diagram of this generic model, we find large parameter regions that support ground states with continuous degeneracies. Due to the spin-orbit entanglement, the generic model does not have any continuous symmetry. The continuous degeneracy is thus accidental and not related to any microscopic symmetry of the model. We expect that, the quantum fluctuations should break the accidental degeneracy and favor magnetic ordered states. This mechanism is known as order by quantum disorder (ObQD)<sup>36,46-48</sup>. Because of the continuous degeneracy, the fluctuations within the degenerate mean-field ground state manifold are very soft and are characterized by the pseudo-Goldstone mode with a nearly gapless dispersion when the system becomes ordered. The pseudo-Goldstone mode is a direct consequence of the ObQD, and the consequence of the nearly gapless pseudo-Goldstone mode is a  $T^3$  temperature dependence of the heat capacity in the ordered phases. In addition to the pseudo-Goldstone mode, the Weyl magnon mode<sup>49</sup> is found in the magnetic excitation for certain magnetic order. In contrast to the low energy pseudo-Goldstone mode, the Weyl magnon mode appears at finite energies due to the bosonic nature of the spin wave excitation.

This paper is organized as follows. In Sec. II, we derive the generalized Kitaev-Heisenberg model. We present a systematic analysis of the mean-field phase diagram of this model in Sec. III. Competition between different interactions, together with the geometrical frustration, leads to a very rich phase diagram. Specifically, among different phases, we focus on the regions with a continuous  $U(1)$  or  $O(3)$  degeneracy, in Sec. IV. The degeneracy at the mean-field level is lifted when the quantum fluctuation is included, and various magnetic orders are favored in these regions. We demonstrate the ObQD explicitly. We further show the magnetic excitations of the resultant ordered phases are characterized by the pseudo-Goldstone mode with a nearly gapless dispersion. Finally, we conclude with a discussion in Sec. V.

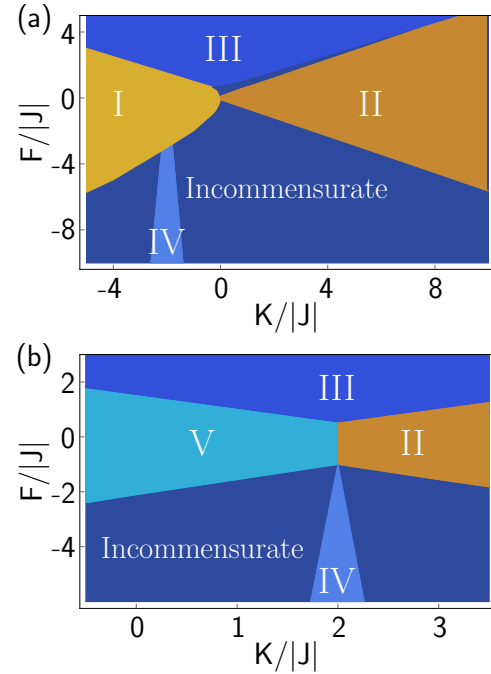


FIG. 2. (Color online.) The mean-field phase diagrams for an antiferromagnetic Heisenberg coupling (a) and for a ferromagnetic Heisenberg coupling (b). The incommensurate phase has non-uniform spin amplitudes on every site. Both phase I and phase II have antiferromagnetic collinear orders with the wavevector  $\mathbf{X}$ , and a continuous  $U(1)$  ground state degeneracy exists in phase II. Both phase III and phase IV have antiferromagnetic collinear orders with the wavevector  $\mathbf{L}$ , and phase IV shows a  $U(1)$  degeneracy. Phase V is ferromagnetically ordered with an  $O(3)$  ground state degeneracy. See the main text and Tab. I for a detailed discussion.

## II. THE GENERALIZED KITAEV-HEISENBERG MODEL

We focus on a series of double perovskite-type oxides<sup>40</sup>,  $\text{Ba}_2\text{LnSbO}_6$  ( $\text{Ln} = \text{rare earth}$ ), where the Ba ions are located at the A sites of the perovskite-type oxides  $\text{ABO}_3$ , and the Ln and Sb ions are regularly ordered at the B sites. Specifically, the Ln and Sb ions are ordered in the rock-salt type structure, with space group  $\text{Fm}\bar{3}\text{m}$ . Each of the two kinds of ions forms a separate FCC lattice. The magnetic behavior depends on the  $\text{Ln}^{3+}$  ions ( $[\text{Xe}]4f^n$ ,  $[\text{Xe}]$ : electronic xenon core), where the SOCs are typically quite large. We study the Kramers' doublet that is formed by the  $4f$  electrons of the  $\text{Ln}^{3+}$  ion with an odd  $n$  when the crystal electric field enters.

Under the  $\text{Fm}\bar{3}\text{m}$  space group symmetry, the pseudospin,  $\mathbf{S}$ , that acts on the Kramers' doublet of the rare earth ion, transforms as a pseudovector. Both the pseudospin position and the pseudospin orientation are transformed. The most general exchange interaction between the local moments on the nearest neighbor sites, allowed by the lattice symmetry, is a generalized Kitaev-

Phase	Wavevector	Order Para.	Continuous deg
I	$(2\pi, 0, 0)$	along [100] axis	–
II	$(2\pi, 0, 0)$	in (100) plane	$U(1)$
III	$(\pi, \pi, \pi)$	along [111] axis	–
IV	$(\pi, \pi, \pi)$	in (111) plane	$U(1)$
V	$(0, 0, 0)$	any direction	$O(3)$

TABLE I. The mean-field phases in Fig. 2. The incommensurate phase is not included here.

Heisenberg model with

$$H = \sum_{\langle ij \rangle_{\gamma\pm}} [J \mathbf{S}_i \cdot \mathbf{S}_j + K S_i^\gamma S_j^\gamma \pm F(S_i^\alpha S_j^\beta + S_i^\beta S_j^\alpha)], \quad (1)$$

where the bond index  $\gamma\pm$  refers to the specific interaction that depends on the orientation of the bond in the plane and the pseudospin components are defined in the global coordinate system (see Fig. 1). We expect the nearest neighbor interaction is sufficient to describe the magnetic properties of the rare-earth moments in this system as the  $4f$  electrons are very localized spatially. Besides the ordinary isotropic Heisenberg exchange interaction, we have the well-known Kitaev exchange interaction as well as the symmetric pseudo-dipole interaction that depends on the bond orientation. In Eq. 1, the antisymmetric Dzyaloshinskii-Moriya interaction is prohibited by the inversion symmetry of the system<sup>50</sup>. The component  $\gamma$  ( $= x, y, z$ ) specifies the three distinct types of Ising coupling in the Kitaev exchange ( $K$  term), and  $\{\alpha, \beta, \gamma\}$  is a cyclic permutation of  $\{x, y, z\}$ , that contributes to the symmetric pseudo-dipole interaction ( $F$  term). The bond dependent pseudospin interaction is a direct consequence of the spin-orbit entanglement and widely occurs in many strong spin-orbit-coupled materials<sup>1,21,26,27,38</sup>.

Compared with the rare-earth triangular system<sup>37,38,51</sup> and the pyrochlore system<sup>30,32,34</sup>, there are only three independent pseudospin interactions in Eq. 1. It is the symmetries of the FCC lattice that help reduce the number of independent pseudospin interactions in our model. This result indicates that one may find even simpler models in strong spin-orbit-coupled systems with large lattice symmetries.

### III. MEAN-FIELD PHASE DIAGRAM

We now discuss the mean-field phase diagram of the generalized Kitaev-Heisenberg model in Eq. 1. We systematically analyze the mean-field ground states in different parameter regimes. We consider both antiferromagnetic and ferromagnetic Heisenberg interactions with  $J > 0$  and  $J < 0$ , respectively.

In the classical mean-field theory, we first treat the pseudospin as a classical vector that satisfies the hard constraint  $|\mathbf{S}_i| = S$ . The classical (mean-field) energy of the system needs to be optimized under this local constraint on every lattice site. This procedure is difficult as

the local hard constraint is hard to implement. Instead, we here adopt the well-known Luttinger-Tisza method<sup>52</sup> that is to replace the local hard spin constraint by a global one such that

$$\sum_i |\mathbf{S}_i|^2 = NS^2, \quad (2)$$

where  $N$  is the total number of the pseudospins in the system. We optimize the classical mean-field energy,

$$E_{\text{cl}} = \sum_{\mathbf{q}} \sum_{\alpha\beta} \mathcal{E}_{\alpha\beta}(\mathbf{q}) S_{\mathbf{q}}^\alpha S_{-\mathbf{q}}^\beta, \quad (3)$$

under the global constraint. Here we have defined

$$S_i^\alpha = \frac{1}{N^{\frac{1}{2}}} \sum_{\mathbf{q}} S_{\mathbf{q}}^\alpha e^{i \mathbf{q} \cdot \mathbf{r}_i}. \quad (4)$$

Once the mean-field ground state satisfies both the global constraint and the local hard spin constraint, then the ground state under this approximation turns out to be the real ground state of the model in the classical limit.

In Fig. 2, we depict the mean-field phase diagram with both antiferromagnetic and ferromagnetic Heisenberg interactions. In the phase diagram, there is a large region where the minimum of the mean-field energy occurs in a set of incommensurate wavevectors (see Fig. 2). In these incommensurate regions, only one spin component is involved in the mean-field ground state. As a result, this incommensurate state cannot satisfy the local hard spin constraint due to the incommensurability. This result indicates the strong frustration in these regions of the generalized Kitaev-Heisenberg model.

We continue with other ordered phases in the phase diagram. In Fig. 2a, phase I is an antiferromagnetic state with the ordering wavevector at  $\mathbf{X} = (2\pi, 0, 0)$  or equivalently  $(0, 2\pi, 0)$ ,  $(0, 0, 2\pi)$ . In this state, the spins order in a collinear pattern. For the  $(2\pi, 0, 0)$  ordering wavevector, the spin ordering is locked to the  $\hat{x}$  direction with,

$$\text{I: } \mathbf{S}_i \equiv S \hat{m}_i = S \hat{x} e^{2\pi x_i}, \quad (5)$$

where  $x_i$  is the  $x$  coordinate of the lattice site  $\mathbf{r}_i$ . The locking between the ordering wavevector and the spin orientation is a direct consequence and general phenomenon of the strong spin-orbit-coupled magnets.

In phase II with a dominant and antiferromagnetic Kitaev interaction ( $K > 0$ ), the system also orders with the wavevector  $\mathbf{X}$  and equivalent ones. Although having the same ordering wavevector, the ground state of phase II has a continuous  $U(1)$  degeneracy. If we choose the  $(2\pi, 0, 0)$  ordering wavevector, the ground state is parameterized as

$$\text{II: } \mathbf{S}_i \equiv S \hat{m}_i = S [\cos \theta \hat{y} + \sin \theta \hat{z}] e^{2\pi x_i}, \quad (6)$$

where  $\theta$  is an angular variable. This  $U(1)$  degeneracy can be well understood, because the classical energy gained from the antiferromagnetic  $K$  term remains invariant

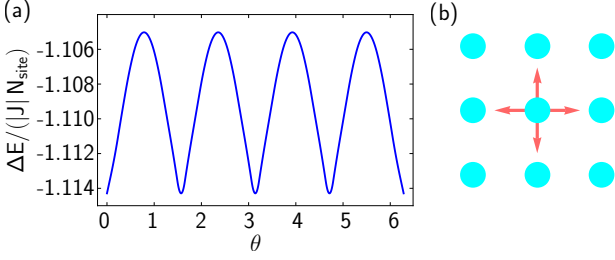


FIG. 3. (Color online.) Quantum zero point energy in  $X = (2\pi, 0, 0)$  ordered state (phase II). (a) The minimum of  $\Delta E$  occurs at  $\theta = n\pi/2$  with  $n \in \mathbb{Z}$ . (b) Arrows indicate four-fold symmetry equivalent pseudospin orientation in the  $(100)$  plane. We choose  $(J, K, F) = (1, 1, 0)$ .

when spin vectors are rotated within the  $U(1)$  manifold. Here the presence of a weak pseudo-dipole interaction does not lift the degeneracy. At the mean field level, phase I and phase II are understood as the easy axis along the  $[100]$  direction and easy plane anisotropy in the  $(100)$  plane for the order parameter, respectively. Note that in region II there also exists a line degeneracy from  $X$  to  $W$  in the reciprocal space. Since only one spin component is involved, therefore, however, it can not form a normalized spin spiral order.

In the regimes dominated by the pseudo-dipole interaction ( $F$  term), we obtain two other ordered phases. Phase III is an antiferromagnetic ordered phase with the ordering wavevector  $L = (\pi, \pi, \pi)$  or equivalent ones. Given  $L = (\pi, \pi, \pi)$ , the spin ordering is locked to the  $[111]$  direction with

$$\text{III: } \mathbf{S}_i \equiv S \hat{m}_i = \frac{S}{\sqrt{3}} (\hat{x} + \hat{y} + \hat{z}) e^{i\pi(x_i + y_i + z_i)}. \quad (7)$$

Finally, phase IV has the same ordering wavevector as phase III but has a  $U(1)$  ground state degeneracy. For the  $(\pi, \pi, \pi)$  ordering, the spin vector is parameterized as

$$\text{IV: } \mathbf{S}_i \equiv S \hat{m}_i = S (\cos \theta \hat{u}_1 + \sin \theta \hat{u}_2) e^{i\pi(x_i + y_i + z_i)}, \quad (8)$$

where  $\theta$  is an angular variable, and  $\hat{u}_1, \hat{u}_2$  are two unit vectors in the  $(111)$  plane, chosen as  $\hat{u}_1 = [1\bar{1}0]/\sqrt{2}$ ,  $\hat{u}_2 = [11\bar{2}]/\sqrt{6}$ . At the mean field level, phase III and Phase IV can be understood as the easy axis along the  $[111]$  direction and easy plane anisotropy in the  $(111)$  plane of the order parameter, respectively. Furthermore, like the case in phase II, a line degeneracy exists in the reciprocal space, from  $L$  to another equivalent  $L$  (e.g. from  $(\pi, \pi, \pi)$  to  $(\pi, \pi, -\pi)$ ). Since the spins do not have uniform magnitudes, they cannot be the ground states.

When the Kitaev interaction is switched to ferromagnetic with  $K < 0$  and remains dominant, the ground state depends on the sign of the Heisenberg interaction. The case with an antiferromagnetic Heisenberg interaction gives phase I. For the ferromagnetic Heisenberg interaction with  $J < 0$ , however, the classical ground state is a simple ferromagnetic state (phase V) but has an  $O(3)$

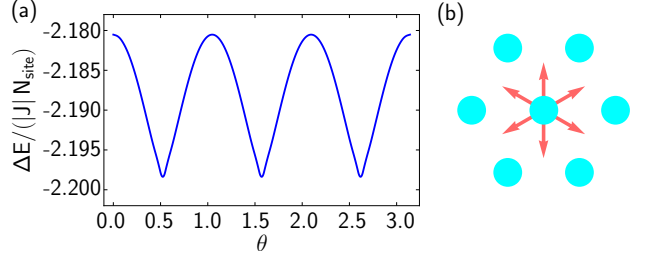


FIG. 4. (Color online.) Quantum zero point energy in  $L = (\pi, \pi, \pi)$  ordered state (phase IV). (a) The minimum of  $\Delta E$  occurs at  $\theta = \pi/6 + n\pi/3$  with  $n \in \mathbb{Z}$ . (b) Arrows indicate six-fold symmetry equivalent pseudospin orientation in the  $(111)$  plane. We choose  $(J, K, F) = (-1, 2, -4)$ .

degeneracy. The spin order is parametrized by two angular variables,

$$\text{V: } \mathbf{S}_i \equiv S \hat{m}_i = S (\sin \theta \cos \phi \hat{x} + \sin \theta \sin \phi \hat{y} + \cos \theta \hat{z}), \quad (9)$$

where  $\theta$  runs from 0 to  $\pi$ , and  $\phi$  runs from 0 to  $2\pi$ . The  $O(3)$  degeneracy, as in the previous  $U(1)$  degeneracy case, is understood from the invariance of the dominant classical energy from the ferromagnetic Kitaev interaction.

As we summarize in Tab. I, these five ordered phases have rather different order parameters. The phase transition between them, if there exists a direct transition between them, is first order.

#### IV. QUANTUM FLUCTUATION AND MAGNETIC EXCITATION

We focus on the ordered phases with a continuous ground state degeneracy, and discuss the role of quantum fluctuation when the quantum nature of the pseudospin is considered. Since the microscopic Hamiltonian only has discrete lattice symmetries, the continuous degeneracy of the mean-field ground states is not granted at the quantum level. We, therefore, expect that the degeneracy in the mean-field level will be lifted when quantum fluctuation is included. Within the linear spin wave theory, we now discuss this order by quantum disorder (ObQD) effect explicitly.

For the ground state with a continuous  $U(1)$  degeneracy, parameterized as in Eq. 6 and Eq. 8, we introduce the Holstein-Primakoff bosons to express the spin operators as

$$\mathbf{S}_i \cdot \hat{m}_i = S - b_i^\dagger b_i, \quad (10)$$

$$\mathbf{S}_i \cdot \hat{n}_i = \frac{(2S)^{\frac{1}{2}}}{2} (b_i + b_i^\dagger), \quad (11)$$

$$\mathbf{S}_i \cdot (\hat{m}_i \times \hat{n}_i) = \frac{(2S)^{\frac{1}{2}}}{2i} (b_i - b_i^\dagger), \quad (12)$$

where  $\hat{m}_i$  is the unit vector describing the spin orientation of classical spin order at site  $i$ ,  $\hat{n}_i$  is a unit vector

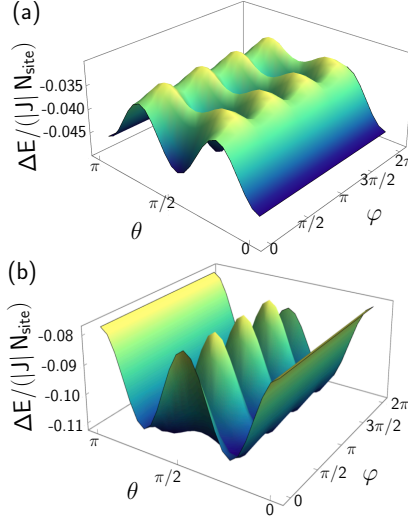


FIG. 5. (Color online.) Quantum zero point energy of two representative parameters in mean-field phase V. The two-dimensional sphere is parametrized by polar angle  $\theta$  and azimuthal angle  $\varphi$ . (a) We set  $(J, K, F) = (-1, 1, 0)$  for phase  $V_a$  in Fig. 6, the favored spin orientations are  $\pm\hat{x}$ ,  $\pm\hat{y}$ , and  $\pm\hat{z}$ , corresponding to the six minima of  $\Delta E$ . (b) We set  $(J, K, F) = (-1, 0, 1)$  for phase  $V_b$  in Fig. 6, the favored spin orientations are  $[111]$  directions, corresponding to the eight minima of  $\Delta E$ .

normal to  $\hat{m}_i$ , and  $S = 1/2$ . We substitute the spin operators with these Holstein-Primakoff bosons. In the linear spin wave approximation, we keep the boson terms up to the quadratic order. The resulting linear spin wave Hamiltonian has the following form

$$H_{\text{sw}} = \sum_{\mathbf{k}} \left[ \sum_{\mu, \nu} (A_{\mu\nu}(\mathbf{k}) b_{\mathbf{k}\mu}^\dagger b_{\mathbf{k}\nu} + B_{\mu\nu}(\mathbf{k}) b_{-\mathbf{k}, \mu} b_{\mathbf{k}\nu} + B_{\mu\nu}^*(-\mathbf{k}) b_{\mathbf{k}\mu}^\dagger b_{-\mathbf{k}, \nu}^\dagger) + C(\mathbf{k}) \right] + E_{\text{cl}}, \quad (13)$$

where  $E_{\text{cl}}$  is the classical mean-field energy of the ground state and independent of the angular variable  $\theta$  due to the  $U(1)$  degeneracy,  $A_{\mu\nu}$ ,  $B_{\mu\nu}$  and  $C$  depend on  $\theta$ , and  $A_{\mu\nu}$ ,  $B_{\mu\nu}$  satisfy

$$A_{\mu\nu}(\mathbf{k}) = A_{\nu\mu}^*(\mathbf{k}), \quad (14)$$

$$B_{\mu\nu}(\mathbf{k}) = B_{\nu\mu}(-\mathbf{k}). \quad (15)$$

While the classical mean-field energy  $E_{\text{cl}}$  preserves the  $U(1)$  degeneracy, the quantum fluctuation lifts this continuous degeneracy through the quantum zero point energy  $\Delta E$  that is given by

$$\Delta E = \sum_{\mathbf{k}} \left[ \sum_{\mu} \frac{1}{2} (\omega_{\mu}(\mathbf{k}) - A_{\mu\mu}(\mathbf{k})) + C(\mathbf{k}) \right], \quad (16)$$

where  $\omega_{\mu}(\mathbf{k})$  is the excitation energy of the  $\mu$ -th spin wave mode at momentum  $\mathbf{k}$ .

In phase II where there is a  $U(1)$  degeneracy (see Eq. 6), the minima of zero point energy  $\Delta E$  occurs at

$$\text{II: } \theta = \frac{n\pi}{2}, \quad (17)$$

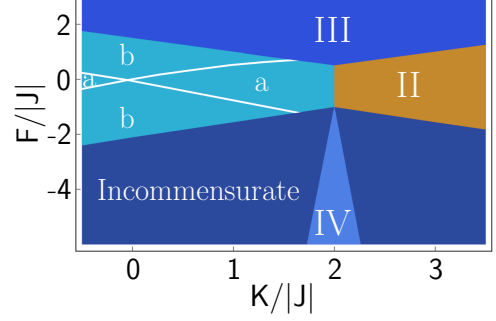


FIG. 6. (Color online.) Phase V in the mean-field phase diagram of Fig. 2 (b) is split into two phases with different magnetic orders once the quantum fluctuation is considered. Here  $J < 0$ .

where  $n \in \mathbb{Z}$ , and the favored magnetic order has a four-fold symmetry equivalent configuration that is shown in Fig. 3.

In phase IV where there is also  $U(1)$  degeneracy (see Eq. 8), the minima of zero point energy  $\Delta E$  occurs at

$$\text{IV: } \theta = \frac{\pi}{6} + \frac{n\pi}{3}, \quad (18)$$

where  $n \in \mathbb{Z}$  and the favored magnetic order has a six-fold symmetry equivalent configuration that is shown in Fig. 4.

Now we turn to phase V of the mean-field phase diagram, the ferromagnetic ordered state with an  $O(3)$  degeneracy. As we have parametrized with a vector on a unit sphere in Eq. 9, two angular variables ( $\theta$  and  $\phi$ ) are needed to capture the  $O(3)$  degeneracy. The minima of the zero point energy  $\Delta E$  are shown in Fig. 5. We find two distinct ordering patterns that are not equivalent under the lattice symmetry. As we depict in Fig. 6, the phase V of the mean-field phase diagram is split into two distinct phases ( $V_a$  and  $V_b$ ). In  $V_a$  ( $V_b$ ), the quantum fluctuation selects the  $[001]$  type ( $[111]$  type) of magnetic order.

The lifting of the  $O(3)$  degeneracy is understood through a cubic anisotropy that is induced by the quantum fluctuation. The cubic anisotropy in the energy is given as

$$E_{\text{ani}} = \lambda_{\text{ani}} [(M^x)^4 + (M^y)^4 + (M^z)^4], \quad (19)$$

where  $\mathbf{M}$  is the order parameter of the ferromagnetic phase. In phase  $V_a$ ,  $\lambda_{\text{ani}} < 0$  and we have the  $[001]$  ordering. In phase  $V_b$ ,  $\lambda_{\text{ani}} > 0$  and we have the  $[111]$  ordering.

Having determined the ground state configurations, we further study the spin wave excitation spectra in different phases. The results are depicted along high symmetry momentum lines in Fig. 7. There are two qualitative features in the spin wave spectra. First, we observe gapless modes in Fig. 7 (a), (b) and (c). These pseudo-Goldstone modes are characteristic of the phase ordered

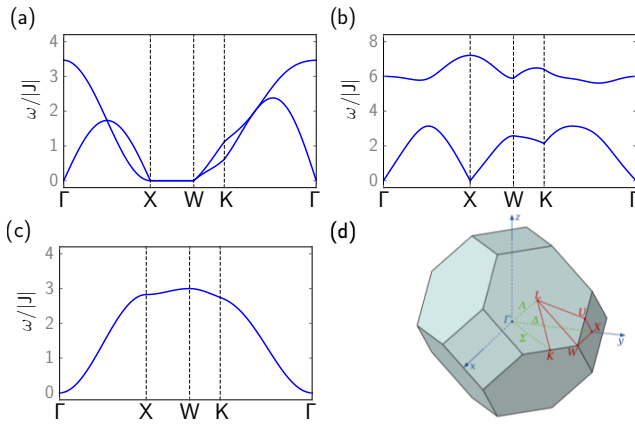


FIG. 7. (Color online.) The representative spin wave spectra along high symmetry momentum lines with (a)  $(J, K, F) = (1, 1, 0)$  and  $\theta = 0$  in phase II; (b)  $(J, K, F) = (-1, 2, -4)$ ,  $\theta = \pi/6$  in phase IV; (c)  $(J, K, F) = (-1, 1, 0)$ ,  $\theta = \pi/2$ ,  $\varphi = 0$  in phase V<sub>a</sub>. In (d) we depict the FCC Brillouin zone (the figure is adapted from Wikipedia<sup>54</sup>).

due to quantum fluctuation that lifts the continuous degeneracy, in our case, phase II, IV and V. Although a small gap is expected to be generated by anharmonic effects, nearly gapless dispersion is a possible experimental signature of the order by quantum disorder scenario. Second, magnon spectrum in Fig. 7 (a) shows band touching (along K- $\Gamma$ ) due to accidental degeneracy, indicating the “Weyl magnon” behavior and the corresponding topologically robust surface states, although the Weyl node along K- $\Gamma$  belong to the type-II node<sup>53</sup> for the specific parameter choice in Fig. 7 (a).

## V. DISCUSSION

Despite the abundance of the rare-earth double perovskites<sup>40,41</sup>, the experimental characterization of them is quite limited. Only the crystal structure and the magnetic susceptibility measurements have been carried out so far. All these compounds are paramagnetic and have no magnetic ordering down to 1.8K<sup>40</sup>. This result does not mean all of them would be spin liquids. The temperature (1.8K) is not quite low for the rare-earth local moments since the exchange interaction between them is of the order of a couple Kelvin. It is very likely that the

absence of magnetic ordering down to 1.8K is a thermal effect, and one could observe the ground state properties if the temperature is further lowered.

What would be the experimental phenomena that are expected for the ObQD phenomena and Weyl magnons? Clearly, one should observe one of the orders that we predict. Moreover, the consequence of the ObQD is the presence of the nearly gapless pseudo-Goldstone mode for the magnetic excitation. Strictly speaking, the pseudo-Goldstone mode should develop a minigap due to the quantum effect, but one would expect a  $T^3$  heat capacity in the temperature regime above the minigap energy scale. For the Weyl magnons, one could probe the spin wave spectrum with the inelastic neutron scattering measurement and directly detect the linear band touching. Alternatively, one could measure the consequence of Weyl magnons, such as the chiral surface state and optical conductivities. All these probes have been discussed in details in Ref. 49.

In many systems, the ObQD is very fragile because other small interactions, that are not included in the model, may simply drive the system into a different state. For rare-earth double perovskites, however, we expect the dominant interaction is from the nearest neighbors. The further neighbor exchanges are rather weak due to the spatial localization of the 4f electrons. The remaining interaction is the magnetic dipole interaction that decays very fast with the separation of the local moments. The actual magnitude would depend on the material’s details such as the the moment size and lattice constants. In any case, we expect the rare-earth double perovskites to be promising candidates for the ObQD phenomena.

The study of the rare-earth double perovskites is in the early stage. Many physical properties of the rare-earth double perovskites need to be measured, and it is very likely that other exotic quantum phases could emerge besides the ones that have been predicted here. We expect our work to bring further attention to this new class of materials.

*Acknowledgements.*—This work is supported by the Start-up funds of Fudan University (Shanghai, People’s Republic of China) and the Thousand-Youth-Talent program (G.C.) of People’s Republic of China. Notes added: we recently get aware that our friend Arun Paramakanti at the Univ of Toronto (Ontario, Canada) and Adam Aczel at Oak Ridge National Laboratory have a similar idea on iridates<sup>55,56</sup>. Their results are consistent with ours in the overlapping parts.

\* These two authors contribute equally.

† [gangchen.physics@gmail.com](mailto:gangchen.physics@gmail.com),  
[gchen\\_physics@fudan.edu.cn](mailto:gchen_physics@fudan.edu.cn)

<sup>1</sup> G. Jackeli and G. Khaliullin, “Mott insulators in the strong spin-orbit coupling limit: From heisenberg to a quantum compass and kitaev models,” Phys. Rev. Lett. **102**, 017205 (2009).

<sup>2</sup> J. Chaloupka, G. Jackeli, and G. Khaliullin, “Kitaev-heisenberg model on a honeycomb lattice: Possible exotic phases in iridium oxides  $A_2\text{iro}_3$ ,” Phys. Rev. Lett. **105**, 027204 (2010).

<sup>3</sup> Hong-Chen Jiang, Zheng-Cheng Gu, Xiao-Liang Qi, and Simon Trebst, “Possible proximity of the mott insulating iridate  $\text{na}_2\text{iro}_3$  to a topological phase: Phase diagram of

the heisenberg-kitaev model in a magnetic field," Phys. Rev. B **83**, 245104 (2011).

<sup>4</sup> Jia-Wei Mei, "Possible fermi liquid in the lightly doped kitaev spin liquid," Phys. Rev. Lett. **108**, 227207 (2012).

<sup>5</sup> I. I. Mazin, Harald O. Jeschke, Kateryna Foyevtsova, Roser Valentí, and D. I. Khomskii, "na<sub>2</sub>iro<sub>3</sub> as a molecular orbital crystal," Phys. Rev. Lett. **109**, 197201 (2012).

<sup>6</sup> Itamar Kimchi and Ashvin Vishwanath, "Kitaev-heisenberg models for iridates on the triangular, hyperkagome, kagome, fcc, and pyrochlore lattices," Phys. Rev. B **89**, 014414 (2014).

<sup>7</sup> J. Chaloupka, G. Jackeli, and G. Khaliullin, "Zigzag magnetic order in the iridium oxide na<sub>2</sub>iro<sub>3</sub>," Phys. Rev. Lett. **110**, 097204 (2013).

<sup>8</sup> M. Hermanns, K. O'Brien, and S. Trebst, "Weyl spin liquids," Phys. Rev. Lett. **114**, 157202 (2015).

<sup>9</sup> T. Takayama, A. Kato, R. Dinnebier, J. Nuss, H. Kono, L. S. I. Veiga, G. Fabbris, D. Haskel, and H. Takagi, "Hyperhoneycomb iridate  $\beta$ -li<sub>2</sub>iro<sub>3</sub> as a platform for kitaev magnetism," Phys. Rev. Lett. **114**, 077202 (2015).

<sup>10</sup> Ioannis Rousochatzakis, Johannes Reuther, Ronny Thomale, Stephan Rachel, and N. B. Perkins, "Phase diagram and quantum order by disorder in the kitaev  $K_1 - K_2$  honeycomb magnet," Phys. Rev. X **5**, 041035 (2015).

<sup>11</sup> K. A. Modic, Tess E. Smidt, Itamar Kimchi, Nicholas P. Breznay, Alun Biffin, Sungkyun Choi, Roger D. Johnson, Radu Coldea, Pilanda Watkins-Curry, Gregory T. McCandless, Julia Y. Chan, Felipe Gandara, Z. Islam, Ashvin Vishwanath, Arkady Shekhter, Ross D. McDonald, and James G. Analytis, "Realization of a three-dimensional spinanisotropic harmonic honeycomb iridate," Nat Commun **5** (2014), 10.1038/ncomms5203.

<sup>12</sup> Satoshi Nishimoto, Vamshi M. Katukuri, Viktor Yushankhai, Hermann Stoll, Ulrich K. Roszler, Liviu Hozoi, Ioannis Rousochatzakis, and Jeroen van den Brink, "Strongly frustrated triangular spin lattice emerging from triplet dimer formation in honeycomb li<sub>2</sub>iro<sub>3</sub>," Nat Commun **7** (2016), 10.1038/ncomms10273.

<sup>13</sup> Jeffrey G. Rau, Eric Kin-Ho Lee, and Hae-Young Kee, "Generic spin model for the honeycomb iridates beyond the kitaev limit," Phys. Rev. Lett. **112**, 077204 (2014).

<sup>14</sup> Jie Lou, Long Liang, Yue Yu, and Yan Chen, "Global phase diagram of the extended kitaev-heisenberg model on honeycomb lattice," arXiv preprint 1501.06990 (2015).

<sup>15</sup> Eric Kin-Ho Lee, Jeffrey G. Rau, and Yong Baek Kim, "Two iridates, two models, and two approaches: A comparative study on magnetism in three-dimensional honeycomb materials," Phys. Rev. B **93**, 184420 (2016).

<sup>16</sup> Yogesh Singh, S. Manni, J. Reuther, T. Berlijn, R. Thomale, W. Ku, S. Trebst, and P. Gegenwart, "Relevance of the heisenberg-kitaev model for the honeycomb lattice iridates A<sub>2</sub>iro<sub>3</sub>," Phys. Rev. Lett. **108**, 127203 (2012).

<sup>17</sup> S. K. Choi, R. Coldea, A. N. Kolmogorov, T. Lancaster, I. I. Mazin, S. J. Blundell, P. G. Radaelli, Yogesh Singh, P. Gegenwart, K. R. Choi, S.-W. Cheong, P. J. Baker, C. Stock, and J. Taylor, "Spin waves and revised crystal structure of honeycomb iridate na<sub>2</sub>iro<sub>3</sub>," Phys. Rev. Lett. **108**, 127204 (2012).

<sup>18</sup> SungBin Lee, Eric Kin-Ho Lee, Arun Paramakanti, and Yong Baek Kim, "Order-by-disorder and magnetic field response in the heisenberg-kitaev model on a hyperhoneycomb lattice," Physical Review B **89**, 014424 (2014).

<sup>19</sup> SungBin Lee, Jae-Seung Jeong, Kyusung Hwang, and Yong Baek Kim, "Emergent quantum phases in a frustrated  $J_1$ - $J_2$  heisenberg model on the hyperhoneycomb lattice," Phys. Rev. B **90**, 134425 (2014).

<sup>20</sup> Yoshihiko Okamoto, Minoru Nohara, Hiroko Aruga-Katori, and Hidenori Takagi, "Spin-liquid state in the  $s = 1/2$  hyperkagome antiferromagnet na<sub>4</sub>ir<sub>3</sub>os," Phys. Rev. Lett. **99**, 137207 (2007).

<sup>21</sup> Gang Chen and Leon Balents, "Spin-orbit effects in na<sub>4</sub>ir<sub>3</sub>os: A hyper-kagome lattice antiferromagnet," Phys. Rev. B **78**, 094403 (2008).

<sup>22</sup> Gang Chen and Yong Baek Kim, "Anomalous enhancement of the wilson ratio in a quantum spin liquid: The case of na<sub>4</sub>ir<sub>3</sub>os," Phys. Rev. B **87**, 165120 (2013).

<sup>23</sup> J. A. Sears, M. Songvilay, K. W. Plumb, J. P. Clancy, Y. Qiu, Y. Zhao, D. Parshall, and Young-June Kim, "Magnetic order in  $\alpha$  - rucl<sub>3</sub>: A honeycomb-lattice quantum magnet with strong spin-orbit coupling," Phys. Rev. B **91**, 144420 (2015).

<sup>24</sup> Heung-Sik Kim, Vijay Shankar V., Andrei Catuneanu, and Hae-Young Kee, "Kitaev magnetism in honeycomb rucl<sub>3</sub> with intermediate spin-orbit coupling," Phys. Rev. B **91**, 241110 (2015).

<sup>25</sup> A. Banerjee, C. A. Bridges, J. Q. Yan, A. A. Aczel, L. Li, M. B. Stone, G. E. Granroth, M. D. Lumsden, Y. Yiu, J. Knolle, S. Bhattacharjee, D. L. Kovrizhin, R. Moessner, D. A. Tennant, D. G. Mandrus, and S. E. Nagler, "Proximate kitaev quantum spin liquid behaviour in a honeycomb magnet," Nat Mater **15**, 733–740 (2016).

<sup>26</sup> Gang Chen, Rodrigo Pereira, and Leon Balents, "Exotic phases induced by strong spin-orbit coupling in ordered double perovskites," Phys. Rev. B **82**, 174440 (2010).

<sup>27</sup> Gang Chen and Leon Balents, "Spin-orbit coupling in  $d^2$  ordered double perovskites," Phys. Rev. B **84**, 094420 (2011).

<sup>28</sup> Alexei Kitaev, "Anyons in an exactly solved model and beyond," Annals of Physics **321**, 2 – 111 (2006), january Special Issue.

<sup>29</sup> W. Witczak-Krempa, G. Chen, Y.B. Kim, and L. Balents, "Correlated quantum phenomena in the strong spin-orbit regime," Annual Review of Condensed Matter Physics **5**, 57–82 (2014).

<sup>30</sup> S. H. Curnoe, "Structural distortion and the spin liquid state in tb<sub>2</sub>ti<sub>2</sub>o<sub>7</sub>," Phys. Rev. B **78**, 094418 (2008).

<sup>31</sup> Jason S. Gardner, Michel J. P. Gingras, and John E. Greedan, "Magnetic pyrochlore oxides," Rev. Mod. Phys. **82**, 53–107 (2010).

<sup>32</sup> Shigeki Onoda and Yoichi Tanaka, "Quantum fluctuations in the effective pseudospin- $\frac{1}{2}$  model for magnetic pyrochlore oxides," Phys. Rev. B **83**, 094411 (2011).

<sup>33</sup> SungBin Lee, Shigeki Onoda, and Leon Balents, "Generic quantum spin ice," Phys. Rev. B **86**, 104412 (2012).

<sup>34</sup> Yi-Ping Huang, Gang Chen, and Michael Hermele, "Quantum spin ices and topological phases from dipolar-octupolar doublets on the pyrochlore lattice," Phys. Rev. Lett. **112**, 167203 (2014).

<sup>35</sup> Yao-Dong Li and Gang Chen, "Octupolar quantum spin ice: controlling spinons in a u(1) quantum spin liquid," arXiv preprint 1607.02287 (2016).

<sup>36</sup> Lucile Savary, Kate A. Ross, Bruce D. Gaulin, Jacob P. C. Ruff, and Leon Balents, "Order by quantum disorder in er<sub>2</sub>ti<sub>2</sub>o<sub>7</sub>," Phys. Rev. Lett. **109**, 167201 (2012).

<sup>37</sup> Yuesheng Li, Gang Chen, Wei Tong, Li Pi, Juanjuan Liu, Zhaorong Yang, Xiaoqun Wang, and Qingming Zhang, "Rare-earth triangular lattice spin liquid: A single-crystal

study of ybmrgao4," Physical review letters **115**, 167203 (2015).

<sup>38</sup> Yao-Dong Li, Xiaoqun Wang, and Gang Chen, "Anisotropic spin model of strong spin-orbit-coupled triangular antiferromagnets," Physical Review B **94**, 035107 (2016).

<sup>39</sup> Dmytro Pesin and Leon Balents, "Mott physics and band topology in materials with strong spin-orbit interaction," Nature Physics **6**, 376–381 (2010).

<sup>40</sup> Shumpei Otsuka and Yukio Hinatsu, "Structures and magnetic properties of rare earth double perovskites containing antimony or bismuth  $\text{ba}_2\text{Ln}\text{moo}_6$  ( $\text{Ln}$ =rare earths;  $\text{m}$ =sb, bi)," Journal of Solid State Chemistry **227**, 132141 (2015).

<sup>41</sup> Alo Dutta, P.K. Mukhopadhyay, T.P. Sinha, Dipankar Das, and Saniranjan Shannigrahi, "Structural and magnetic properties of double perovskite oxide  $\text{ba}_2\text{cesbo}_6$ ," Solid State Sciences **58**, 64 – 69 (2016).

<sup>42</sup> Tomoko Aharen, John E. Greedan, Craig A. Bridges, Adam A. Aczel, Jose Rodriguez, Greg MacDougall, Graeme M. Luke, Takashi Imai, Vladimir K. Michaelis, Scott Kroeker, Haidong Zhou, Chris R. Wiebe, and Lachlan M. D. Cranswick, "Magnetic properties of the geometrically frustrated  $s = \frac{1}{2}$  antiferromagnets,  $\text{la}_2\text{limoo}_6$  and  $\text{ba}_2\text{ymoo}_6$ , with the b-site ordered double perovskite structure: Evidence for a collective spin-singlet ground state," Phys. Rev. B **81**, 224409 (2010).

<sup>43</sup> C. R. Wiebe, J. E. Greedan, P. P. Kyriakou, G. M. Luke, J. S. Gardner, A. Fukaya, I. M. Gat-Malureanu, P. L. Russo, A. T. Savici, and Y. J. Uemura, "Frustration-driven spin freezing in the  $s = \frac{1}{2}$  fcc perovskite  $\text{sr}_2\text{mgre}_6$ ," Phys. Rev. B **68**, 134410 (2003).

<sup>44</sup> C. R. Wiebe, J. E. Greedan, G. M. Luke, and J. S. Gardner, "Spin-glass behavior in the  $s = 1/2$  fcc ordered perovskite  $\text{sr}_2\text{care}_6$ ," Phys. Rev. B **65**, 144413 (2002).

<sup>45</sup> A. S. Erickson, S. Misra, G. J. Miller, R. R. Gupta, Z. Schlesinger, W. A. Harrison, J. M. Kim, and I. R. Fisher, "Ferromagnetism in the mott insulator  $\text{ba}_2\text{naoso}_6$ ," Phys. Rev. Lett. **99**, 016404 (2007).

<sup>46</sup> Christopher L. Henley, "Ordering by disorder: Ground-state selection in fcc vector antiferromagnets," Journal of Applied Physics **61**, 3962–3964 (1987).

<sup>47</sup> J. Villain, R. Bidaux, J.P. Carton, and R. Conte, "Order as an effect of disorder," J. Phys. (Paris) **41**, 1263 (1980).

<sup>48</sup> M. E. Zhitomirsky, M. V. Gvozdikova, P. C. W. Holdsworth, and R. Moessner, "Quantum order by disorder and accidental soft mode in  $\text{er}_2\text{ti}_2\text{o}_7$ ," Phys. Rev. Lett. **109**, 077204 (2012).

<sup>49</sup> Fei-Ye Li, Yao-Dong Li, Yong Baek Kim, Leon Balents, Yue Yu, and Gang Chen, "Weyl magnons in breathing pyrochlore antiferromagnets," arXiv:cond-mat/ **1602.04288** (2016).

<sup>50</sup> Tôru Moriya, "Anisotropic superexchange interaction and weak ferromagnetism," Phys. Rev. **120**, 91–98 (1960).

<sup>51</sup> Yao Shen, Yao-Dong Li, Hongliang Wo, Yuesheng Li, Shoudong Shen, Bingying Pan, Qisi Wang, H. C. Walker, P. Steffens, M. Boehm, *et al.*, "Spinon fermi surface in a triangular lattice quantum spin liquid  $\text{YbMgGaO}_4$ ," arXiv preprint 1607.02615 (2016).

<sup>52</sup> J. M. Luttinger and L. Tisza, "Theory of dipole interaction in crystals," Phys. Rev. **70**, 954–964 (1946).

<sup>53</sup> A. A. Soluyanov, D. Gresch, Z. Wang, Q. Wu, M. Troyer, X. Dai, and B. A. Bernevig, "Type-II Weyl semimetals," Nature (London) **527**, 495–498 (2015).

<sup>54</sup> "Brillouin zone," Wikipedia.

<sup>55</sup> A. M. Cook, S. Matern, C. Hickey, A. A. Aczel, and A. Paramekanti, "Spin-orbit coupled  $j_{\text{eff}} = 1/2$  iridium moments on the geometrically frustrated fcc lattice," Phys. Rev. B **92**, 020417 (2015).

<sup>56</sup> A. A. Aczel, A. M. Cook, T. J. Williams, S. Calder, A. D. Christianson, G.-X. Cao, D. Mandrus, Yong-Baek Kim, and A. Paramekanti, "Highly anisotropic exchange interactions of  $j_{\text{eff}} = \frac{1}{2}$  iridium moments on the fcc lattice in  $\text{La}_2\text{BIrO}_6$  (B=Mg,Zn)," Phys. Rev. B **93**, 214426 (2016).